ACCEPTED MANUSCRIPT

Experimental characterisation of the magnetic field correction factor, $\kappa_{\to_B}$, for Roos chambers in a parallel MRI-linac

Title: Experimental characterisation of the magnetic field correction factor, $k_{\vec{B}}$, for Roos chambers in a parallel MRI-linac

Keywords:

absorbed dose, magnetic field, MRgRT, MRI-linacs, Roos Chamber

Authors:

Jarrad Begg[1-3], Urszula Jelen[2], Paul Keall[2,4], Gary Liney[1,2,3,5], Lois Holloway[1-6]

[1]Department of Medical Physics, Liverpool and Macarthur Cancer Therapy Centre, Liverpool, NSW, 2170, Australia

[2]Ingham Institute for Applied Medical Research, Liverpool, NSW, 2170, Australia

[3]South Western Sydney Clinical School, University of New South Wales, Liverpool, NSW, 2170, Australia

[4]Faculty of Medicine and Health, University of Sydney, Camperdown, NSW, 2505, Australia

[5]Centre for Medical Radiation Physics, University of Wollongong, Wollongong, New South Wales (NSW), 2522, Australia

[6]Institute of Medical Physics, University of Sydney, Camperdown, NSW, 2505, Australia

Corresponding Author Email:

jarrad.begg@health.nsw.gov.au

Abstract:

Objective

20 Reference dosimetry on an MRI-linac requires a chamber specific magnetic field correction factor, $k_{\vec{B}}$. This work aims to measure the correction factor for a parallel plate chamber on a parallel MRI-linac.

Approach

$k_{\vec{B}}$ is defined as the ratio of the absorbed dose to water calibration coefficient in the presence of the magnetic field, $N_{D,w}^{\vec{B}}$ relative to that under 0 T conditions, $N_{D,w}^{0T}$. $k_{\vec{B}}$ was measured via a $N_{D,w}$ transfer

25 to a field chamber at each magnetic field strength from a chamber with known $N_{D,w}$ and $k_{\vec{B}}$. This was achieved on the parallel MRI-linac by moving the measurement set-up between a high magnetic field strength region at the MRI-isocentre and a low magnetic field strength region at the end of the bore whilst maintaining consistent set-up and scatter conditions. Three PTW 34001 Roos chambers were investigated as well as a PTW 30013 Farmer used to validate methodology.

Main Results

30 The beam quality used for the measurements of $k_{\vec{B}}$ was $TPR_{20/10}$ = 0.632. The $k_{\vec{B}}$ for the PTW Farmer chamber at 1 T on a parallel MRI-linac was 0.993 ± 0.013 (*k* = 1). The average $k_{\vec{B}}$ factor measured for the three Roos chambers on a 1 T parallel MRI-linac was 0.999 ± 0.014 (*k* = 1).

Significance

35 The results presented are the first measurements of $k_{\vec{B}}$ for a Roos chamber on a parallel MRI-linac. The Roos chamber results demonstrate the potential for the chamber as a reference dosimeter in parallel MRI-linacs.

Introduction

MRI-linacs have been developed with the radiation field aligned perpendicular to the main magnetic

40 field (B_0) (Lagendijk *et al.*, 2014; Mutic and Dempsey, 2014), and with the radiation field aligned

parallel to the B_0 field (Keall *et al.*, 2014; Fallone, 2014). The Lorentz force has the potential to impact

the dose deposition of both systems. For perpendicular MRI-linacs the electrons depositing dose are

more likely to scatter laterally and slightly shallower relative to conventional linacs causing a lateral

shift in the dose deposition (Raaijmakers *et al.*, 2008). Electrons depositing dose on parallel MRI-linacs

45 are more likely to be forward scattered and only the vector component of the electron that is

perpendicular to the magnetic field is affected causing no change in dose deposition provided charged

particle equilibrium is maintained (Bielajew, 1993).

The magnetic field has previously been shown to impact dosimetry measurements due to changes in

the pathlength of electrons across the chamber (Meijsing *et al.*, 2009). Dosimetry measurements on

50 conventional linacs are traceable to primary standards laboratories. A similar traceability is required

for MRI-linacs in order to ensure accuracy of the dose being delivered to patients. Therefore, accurate

magnetic field correction factors, accounting for the change in dose deposition and chamber response,

are required in order to accurately measure dose.

Magnetic field correction factors have been shown to depend on chamber size (Spindeldreier *et al.*,

55 2017) and orientation between the chamber, magnetic field and radiation field (O'Brien *et al.*, 2016;

Malkov and Rogers, 2018; Reynolds *et al.*, 2013; Reynolds *et al.*, 2017; Meijsing *et al.*, 2009; Smit *et

al.*, 2013). The different MRI-linac designs have different radiation beam qualities, magnetic field

strengths and orientations making chamber corrections specific to a system. For perpendicular MRI-

linacs, the magnetic field causes a lateral shift of the electrons inside the sensitive volume. The lateral

60 shift in the electrons not only changes the number of ionisation events detected in the sensitive

volume, but can also cause electrons that would have deposited dose inside the sensitive volume to

deposit dose inside the dead volume of the ionisation chamber or alternatively, cause electrons that

would not have deposited dose inside the sensitive volume to be deflected into the sensitive volume (Pojtinger *et al.*, 2019). For parallel MRI-linacs, electrons in air material have been shown to reduce

65 lateral scatter and increase pathlength parallel to the central axis (Gargett *et al.*, 2015). Minor changes in the dose distribution inside a cylindrical chamber have been simulated(Spindeldreier *et al.*, 2017). Therefore, only small changes in the charge collected inside the sensitive volume of an ion chamber are expected due to the magnetic field.

Chamber correction factors have been simulated for Farmer-type chambers with corrections in the

70 order of 1 % for parallel MRI-linacs (Spindeldreier *et al.*, 2017; Malkov and Rogers, 2018). Previous Monte Carlo simulations of correction factors for parallel plate chambers for perpendicular MRI-linacs have been up to 9 % dependent on magnetic field strength and chamber type (Pojtinger *et al.*, 2018; Malkov and Rogers, 2018). For parallel MRI-linacs, prior simulations have shown correction factors in the order of 1.5 % (Malkov and Rogers, 2018). No measurements of parallel plate correction factors

75 have been presented in the literature and thus no verification of the Monte Carlo simulations. The aim of this work was to measure the correction factor for a parallel plate type chamber on a high field parallel MRI-linac.

Methods

The Australian MRI-Linac

80 The Australian MRI-linac consists of a Varian Linatron (Varian Medical Systems, Inc, USA) radiation source aligned parallel to the primary magnetic field, B_0, of a bespoke 1 T split bore magnet (Agilent Technologies Inc. USA). The radiation source is decoupled from the magnet allowing the radiation source to MRI isocentre distance to change (Jelen *et al.*, 2020). The radiation beam is a flattening filter free (FFF) beam with a beam quality of $TPR_{20/10}$ = 0.632 (Begg *et al.*, 2019). The magnet design

85 incorporates a low field strength region at the end of the MRI bore (Whelan *et al.*, 2018; Roberts *et al.*, 2019).

Magnetic field correction factor formalism

The magnetic field impacts both the dose distribution and the pathlength of electrons through dosimeters, which effects the collected charge. Examples of the change in the dose distribution for

90   perpendicular and parallel fields have been described by Raaijmakers *et al.* (Raaijmakers *et al.*, 2008) and Bielajew (Bielajew, 1993) respectively. Examples of changing electron path lengths through ion chamber cavities has been shown by Meijsing *et al.* (Meijsing *et al.*, 2009).

Dose to water is measured via the charge collected in the dosimeter, corrected for influence quantities, dosimeter calibration factor and beam quality correction factor as shown in equation 1.

95    $D_{w,Q}$ is the dose to water at a certain beam quality, Q. M_Q is the measured charge at the beam quality Q correct for influence factors such as temperature, pressure, polarity and recombination. N_{D,w,Q_0} is the dosimeter calibration factor at the reference beam quality, Q_0. k_{Q,Q_0} is the correction between the reference and measured beam quality.

$$D_{w,Q} = M_Q N_{D,w,Q_0} k_{Q,Q_0} \qquad\qquad (\quad 1 \quad)$$

100   The magnetic field correction factor, $k_{\vec{B}}$, is used during reference dosimetry in a magnetic field to correct for the change in the pathlength of electrons through a detector which affects the measured charge of the detector. The correction factor is the ratio of the dose to water calibration coefficient at the magnetic field strength, $N_{D,w_{Field}}^{\vec{B}}$, relative to no magnetic field, $N_{D,w_{Field}}^{0T}$, at the same beam quality (see equation 2). The correction factor is dependent on the orientation of the chamber, radiation

105   beam and magnetic field, as well as the machine specific reference conditions. Following the nomenclature established by de Pooter *et al.*(de Pooter *et al.*, 2020), the notation $k_{\vec{B}}$ is used in this work. The notation for beam quality, Q, has been removed as the work was completed at the one beam quality.

$$k_{\vec{B}} = \frac{N_{D,w_{Field}}^{\vec{B}}}{N_{D,w_{Field}}^{OT}} \qquad (\quad 2 \quad)$$

110 This study measures the $N_{D,w_{Field}}^{\vec{B}}$ and $N_{D,w_{Field}}^{OT}$ for field chambers via cross-calibration from a detector with known $N_{D,w}$ values at both magnetic field strengths. From this, the $k_{\vec{B}}$ for each chamber was determined.

The dose to water calibration coefficient at each field strength can be broken down into the ratio of the dose to water divided by the measured charge of the chamber. The magnetic field correction

115 factor corrects the response of the detector for the influence of the magnetic field. The magnetic field can affect the detector by changing both the path of the electrons in detector and by changing the electron fluence in the medium around the detector (O'Brien *et al.*, 2016; van Asselen *et al.*, 2018). Dose deposition changes in water are essential to consider when determining the magnetic field correction factor by means of the method applied in the current study. For a parallel orientation MRI-

120 linac, previous simulations (Bielajew, 1993; Oborn *et al.*, 2016) and measurements (Begg *et al.*, 2019) have shown no difference in the absorbed dose at the measurement point. Bielajew (Bielajew, 1993) showed via simulations and mathematical proofs that, provided lateral scatter equilibrium was established, the dose deposited to a point is independent of the magnetic field strength in parallel systems. Therefore the magnetic field influence on dose deposition on parallel MRI-linacs does not

125 need to be considered in the current study. For perpendicular orientation MRI-linacs, the curved path of the electrons due to the magnetic field, causes the energy from a photon interaction point to be deposited, on average, closer to the interaction point. This reduces the absorbed dose at the measurement point by ~ 0.5 % in a 10 cm × 10 cm field at 1.5 T (van Asselen *et al.*, 2018; O'Brien *et al.*, 2016). The measurements presented in this work only considers the parallel geometry.

130 *Magnetic field correction factor measurement overview*

Current available methods of measuring chamber correction factors involve building specific calorimeters for use in magnetic fields (de Prez *et al.*, 2019), alanine dosimetry (Billas *et al.*, 2017) or measuring output during ramp-down and ramp-up states of the magnet (Smit *et al.*, 2013; van Asselen *et al.*, 2018). Monte Carlo calculated chamber correction factors have also been simulated (O'Brien *et*

135 *al.*, 2016; Spindeldreier *et al.*, 2017; Malkov and Rogers, 2018; Reynolds *et al.*, 2013; Pojtinger *et al.*, 2018; Meijsing *et al.*, 2009). Detectors require measurements at both high and low field strengths to directly measure magnetic field correction factors. This leaves two options: 1) A monitor dependent method where the magnet is ramped up and down for measurements at a 0 T and high field strength (van Asselen *et al.*, 2018; Smit *et al.*, 2013), or 2) Move the measurement set-up between the high

140 and low magnetic field strength regions so that measurements are acquired with the chamber at each field region whilst maintaining irradiation conditions such as consistent field size, detector depth and source to surface distance. The decoupled nature of the radiation source and magnet on the Australian MRI-linac allows the second approach to be applied in this work.

The monitor dependent method, used by van Asselen *et al.* (van Asselen *et al.*, 2018) to determine $k_{\vec{B}}$,

145 separates the magnetic field effects on dose deposition and detector response. The dose deposition difference was assessed via Monte Carlo simulations and detector response via the ramping up and down of the magnetic field. Our method for determining $k_{\vec{B}}$ combines the difference in dose deposition and detector response into the $N_{D,w}$ transfer at each field strength.

The $k_{\vec{B}}$ was measured via a cross calibration of the absorbed dose to water calibration coefficient, $N_{D,w}$

150 , between a reference and field chamber, in both the high and low magnetic field set-ups on the Australian MRI-linac to obtain the factors required for the field chamber in equation 1. The reference chamber used in this work was previously calibrated by the National Physics Laboratory (NPL, Teddington, UK) at 0 T via a conventional calibration and at 1 T via Alanine (Billas *et al.*, 2018). Therefore in the high and low magnetic field set-ups the appropriate $N_{D,w}$ was transferred. The

155 reference chamber was a Scanditronix Wellhofer FC65-G (IBA Dosimetry GmbH, Schwarzenbruck,

Germany). The separate 0 T and 1 T $N_{D,w}$ calibration of this chamber results in a $k_{\vec{B}}$ of 0.990 ± 0.012 on the Australian MRI-linac using equation **Error! Reference source not found.**. This value agrees well with the previously simulated value of 0.9914 ± 0.001 which was for a parallel 7 MV photon beam and a 1.5 T magnetic field (Malkov and Rogers, 2018).

160   Figure 1A shows the measurement set-up for a Roos chamber (PTW-Freiburg GmbH, Freiburg, Germany) at the low magnetic strength field region at the end of the magnet bore. Figure 1B shows a diagram of the low and high field measurement set-ups highlighting the consistent source to chamber distance maintained between the two set-ups. A $N_{D,w}$ transfer was used for the measurements in the low and high field region due to the output of the linatron changing with source to MRI-isocentre

165   distance due to the impact of the fringe field (Jelen *et al.*, 2020).
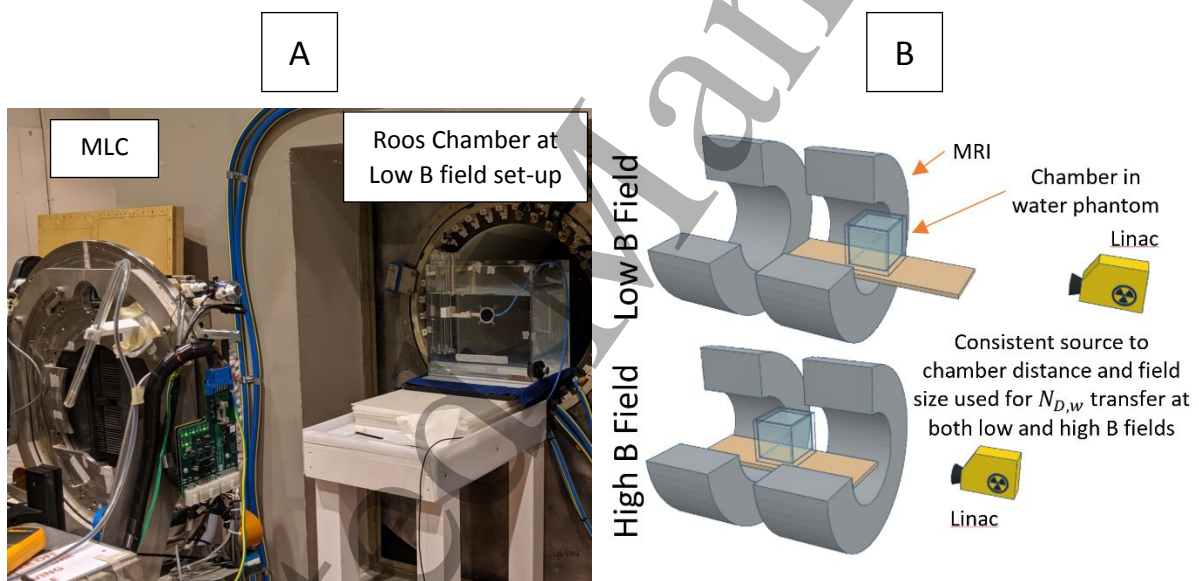
Figure 1: A) A Roos chamber set-up at the low magnetic field strength region. B) Diagram of the chamber, linac and MRI for both the low and high field measurement set-ups. The measurement set-up was transferred between the low and high field region maintaining consistent source to chamber distances and field sizes.

170   The method used to measure $k_{\vec{B}}$ requires the low field region at the end of the bore to be identified so that consistent conditions can be maintained between the high and low field set-ups. The method was validated by measurement of the correction factor for a second Farmer-type chamber which could

be compared to published factors from the literature. Once validated, $k_{\vec{B}}$ for three Roos chambers

were measured and compared to the literature. Three Roos chambers were measured in this work to

175 investigate agreement between the chambers.

Detectors

The Farmer-type chambers were a Scanditronix Wellhofer FC65-G (s/n: 819) and a PTW 30013 0.6cc

(s/n: 10066). The FC65-G was used as the reference as a calibration traceable to the NPL had been

established. The reference point of the Farmer-type chambers (central axis) was set up at 10 cm depth

180 in water.

The magnetic field correction factor was measured for three PTW 34001 Roos chambers (s/n: 473,

1394 and 2957). The inside surface of the entrance window of the Roos chambers was set up at 10 cm

depth in water.

A CC13 chamber (s/n: 15996, IBA Dosimetry GmbH) was set up as an external monitor chamber

185 between the source and MLC to correct for variations in linac output within repeat measurements.

The external monitor chamber was used to correct linac output between different chambers at each

magnetic field but was not used to correct output between magnetic field strengths as this

independent monitor would be subject to changing magnetic field conditions as the linac was moved

between the low and high field measurement set-ups.

190 *Low B Field Location for chamber measurements*

Simulations of the magnetic field map for the MRI used as part of the Australian MRI-Linac, showing

both the low and high magnetic field strength positions, have been presented by Whelan *et al.*

(Whelan *et al.*, 2018) and Roberts *et al.* (Roberts *et al.*, 2019). Previous measurements of the magnetic

field near the low magnetic field point have shown magnetic field strengths less than 0.05 T. To

195 identify the position of the minimum magnetic field strength, and therefore the optimal location for

the placement of the chamber, as well as evaluate uncertainties associated with incorrect positioning

of the detectors at the low field region, the magnitude of the magnetic field strength position was mapped in a 2D plane at isocentre height from the isocentre out to a distance of 250 cm towards the radiation source. A single direction HGM09s Gaussmeter (MAGSYS, Germany, s/n: 011215007) was used in the MRI-linac bore and a Vector/Magnitude 140 Gaussmeter Model VGM (s/n: 568, AlphaLab Inc, Utah, USA) outside the bore.

Measurements of $k_{\vec{B}}$

The $k_{\vec{B}}$ for all chambers was calculated based on the average of the $k_{\vec{B}}$ measured for each chamber in three separate transfer sessions. A singular transfer session consisted of transferring the dose to water calibration coefficient, at both magnetic field strengths, from the FC65-G chamber to the new chamber (either the PTW Farmer or one of the three Roos chambers). Polarity and recombination were measured for each chamber at both magnetic field strengths. Measured charge for each chamber was corrected for temperature, pressure, polarity and recombination via established methods (Andreo *et al.*, 2001). The transfer session was repeated three times on separate days to investigate set-up reproducibility and the stability of polarity, recombination and $k_{\vec{B}}$. Measured transfers of the dose to water calibration coefficient at each magnetic field were assessed for reproducibility over the three separate measurements. The average dose to water calibration coefficient for each magnetic field strength was then used in equation 1 to calculate the magnetic field correction factor, $k_{\vec{B}}$. An uncertainty budget for the measurement of $k_{\vec{B}}$ is detailed below.

Recombination and polarity were measured at the low and high magnetic field strength set-ups to determine if the magnetic field would influence chamber characteristics. Jaffe plots, over a voltage range of 50 V – 300 V for the Farmer-type and 25 V – 150 V for the Roos chambers, were used to compare the charge collected and the applied polarity voltage to determine if the magnetic field had an impact on the suitability of the applied voltage range for determining recombination via the two voltage method.

The measured $k_{\vec{B}}$ for the PTW Farmer was compared to simulations from Malkov and Rogers (Malkov and Rogers, 2018) and Spindeldreier *et al.* (Spindeldreier *et al.*, 2017) in order to validate the proposed measurement methodology.

Rotational Response of the Roos Chamber

225 Rotations of the front face of the Roos chamber away from perpendicular to the beam central axis were measured at both field strengths to investigate the impact of angular set-up uncertainties on $k_{\vec{B}}$. 0° angle was defined as the front face of the Roos chamber perpendicular to the beam/magnetic field direction. Angular response measurements consisted of the following at both the low and high field: 1) An initial chamber response with the chamber set-up at a 0° angle, 2) Chamber response readings

230 at 10 degree intervals in a positive or clockwise rotation to + 30°, 3) Repeat chamber response measurement at 0° angle, 4) Chamber response readings at 10 degree intervals in a negative or counter-clockwise rotation to - 30°, 5) Repeat chamber response measurement at 0° angle. The response at each angle was calculated relative to the average response at 0° for each magnetic field strength. The difference between low and high magnetic field responses at the same angle were

235 compared. Three repeat angular response data sets were acquired for the Roos chamber with serial number 2957 to assess reproducibility.

Calculation of Uncertainties

The uncertainty of $k_{\vec{B}}$ measured via a $N_{D,w}$ transfer at both low and high field strength was calculated via a full uncertainty budget (JCGM, 2008). First the combined relative standard uncertainty of the

240 $N_{D,w}$ transfer for both the PTW Farmer chamber and Roos chamber at both 0 T and 1 T was evaluated. Second, the combined relative standard uncertainty of the transferred $N_{D,w}$ at each magnetic field strength was then used to calculate the combined relative standard uncertainty in $k_{\vec{B}}$ for each chamber (Table 1). A Type A interday reproducibility of the measured $k_{\vec{B}}$ was also included in the combined relative standard uncertainty. For both Farmer-type and Roos chambers the combined

245 relative standard uncertainty in the measured $k_{\vec{B}}$ was 1.6 % (k = 1).

Considered in the combined relative standard uncertainty of the $N_{D,w}$ transfer were the reproducibility of the reference and field chambers, uncertainty in the $N_{D,w}$ value from the NPL, positioning of the reference and field chamber at the correct depth, water tank set-up distance, stability of the reference chamber over time and uncertainty in the influence quantities (temperature, pressure, polarity, recombination and leakage). Differences in the radial profile between the two Farmer-type chambers were not considered as the cross-section of the chamber is of approximately the same size. Differences in the radial profile between the Roos chamber and the Farmer-type reference chamber were evaluated via calculation of the non-uniformity correction along both the long and lateral axes of the Farmer-type chamber and the corresponding axes for the Roos chamber. An estimation in the uncertainty due to differences in volume averaging between the Farmer-type and Roos chambers was given based on the observed differences in the non-uniformity correction. Differences in the non-uniformity correction were observed to be small due to the extended set-up distance of the FFF beam minimising differences in the radial profile. Measurements in this work show that rotations of the Roos chamber of greater than 10° are required to impact the measured charge. Set-up of the Roos chamber restricted rotations to 1° - 2°. Therefore, rotational positional uncertainty of the Roos chamber was considered negligible and not included in the uncertainty budget. Details on the combined relative standard uncertainty of the $N_{D,w}$ transfer are described in appendix table 1.

Table 1: Combined relative standard uncertainty of the $N_{D,w}$ transfer at both 0 T and 1 T for the PTW Farmer and Roos chambers.

Component of Uncertainty	PTW Farmer (%)	Roos (%)
Type A		
Interday Reproducibility of $k_{\vec{B}}$ for each chamber	0.04	0.2
Type B		
Uncertainty in $N_{D,w,Q}$ for chamber at 0 T (see Appendix Table 1**Error! Reference source not found.**)	0.8	0.85

Uncertainty in $N_{D,w,Q}$ for chamber at 1 T (see Appendix Table 1**Error! Reference source not found.**)	1.1	1.1
Combined Relative Standard Uncertainty (k = 1)	1.34 %	1.4 %
Expanded Uncertainty (k = 2)	2.7 %	2.8 %

265

Results

Low B Field Location for chamber measurements

The minimal B field location identified for optimal chamber position at the low magnetic field region was measured to be 0.001 T in magnitude at a distance from the MRI isocentre of 129 cm. The

270   magnitude of the magnetic field was less than 0.007 T in volume of 1 cm radius surrounding the low magnetic region.

Measurements of $k_{\vec{B}}$

Measurements of the recombination and polarity were within 0.2 % of unity for the FC65-G and PTW Farmer chambers and 0.3 % of unity for the Roos chambers with no difference between the magnetic

275   fields observed. Jaffe plots, for both the Farmer-type chambers and the Roos chambers, show collected charge following a linear trend over the range of voltages applied. Repeat measurements of the transferred dose to water calibration coefficient for the PTW Farmer were within 0.1 % of the average value at the low and high magnetic field strength respectively. Repeat measurements of the transferred dose to water calibration coefficients for the three Roos chambers were within 0.3 % of

280   the average value at both magnetic field strengths.

The average $k_{\vec{B}}$ for the PTW Farmer chamber was 0.993 ± 0.013 (k = 1). Uncertainty was calculated as per table 1. The measured magnetic field correction factor for each transfer session was within 0.1 % of the average correction factor measured from 3 repeat transfer sessions for the PTW Farmer chamber.

285 The dose to water calibration coefficients measured for two Roos chambers (s/n: 1394 and 2957) were in good agreement with each other for each magnetic field strength. Roos chamber s/n: 473 was systematically 2.5 % – 3 % higher relative to the measured coefficients for Roos chambers with serial numbers 1394 and 2957.

The average measured $k_{\vec{B}}$ for all three Roos chambers was 0.999 ± 0.014 (k = 1). Uncertainty was 290 calculated as per table 1. Figure 2 shows the measured magnetic field correction factor for each transfer session, for all three chambers, was within 0.2 % of the average correction factor.
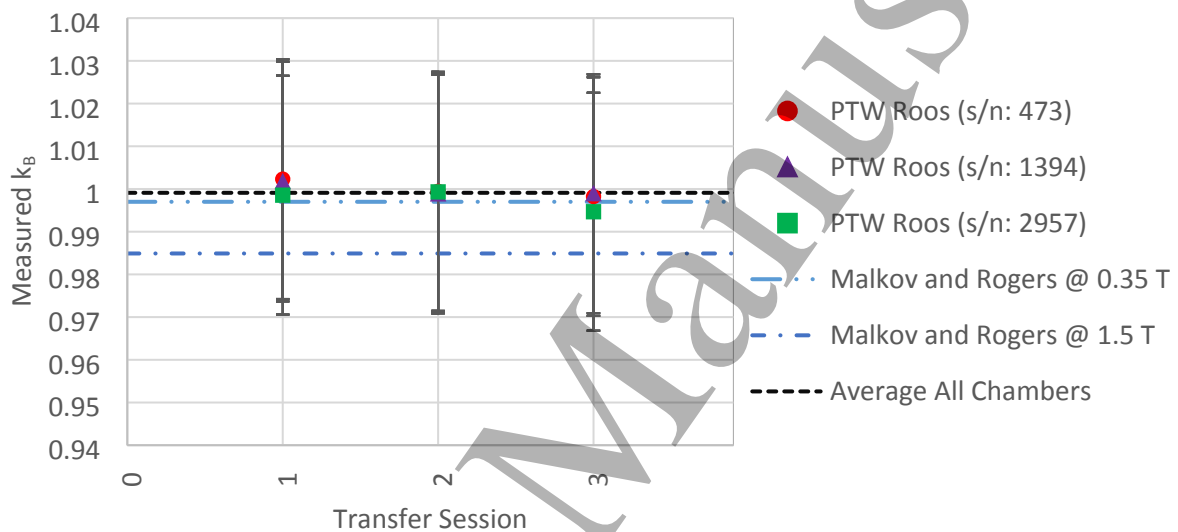
Figure 2: Measured $k_{\vec{B}}$ for the three Roos chambers for the three measurements. The average $k_{\vec{B}}$ over all chambers was 0.999 ± 0.014 (k = 1). $k_{\vec{B}}$ was measured for a parallel MRI-linac at a beam quality 295 of $TPR_{20/10}$ = 0.632. Uncertainty was calculated as per table 1. Error bars around individual $k_{\vec{B}}$ measurements are 95 % confidence intervals (k = 2). The results show agreement with previously published data from Malkov and Rogers (Malkov and Rogers, 2018).

Rotational Response of the Roos Chamber

The response of the three Roos chambers with varying rotational tilt is shown in figure 3. 300 Reproducibility of the chamber response at 0° across the 3 chambers was within ± 0.16 % at both field strengths. The average response of the Roos chamber with a ± 10° face tilt was less than ± 0.2 %

different relative to the response measured with a 0° face tilt at both field strengths. An outlier of - 0.22 % difference relative to 0° was observed for the Roos 473 at an angle of - 10°. The response at high field strengths for non 0° angles relative to the 0° angle was within 0.2 % of the low field strength response for the corresponding angle between ± 30°.
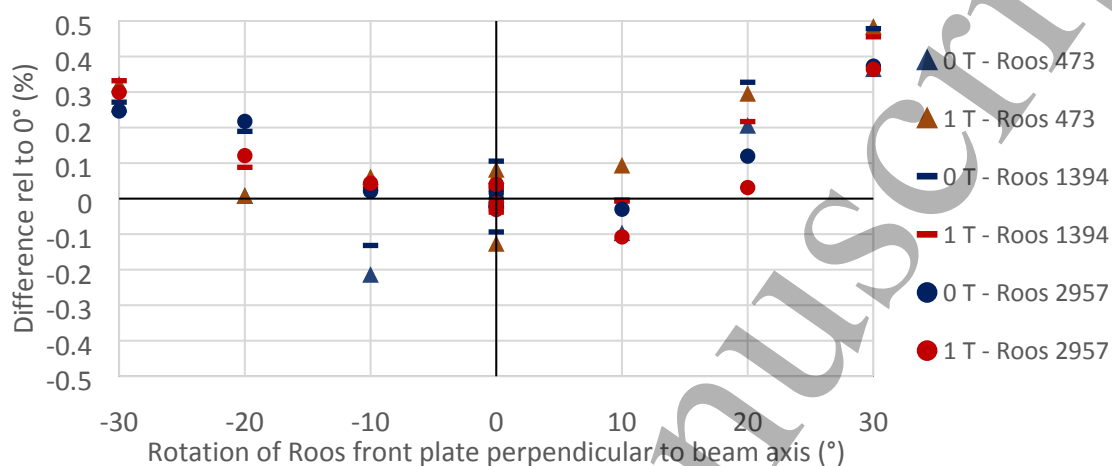

Figure 3: Measured response of the three Roos chambers at different angular rotations relative to an average 0° response

Discussion

In this work we experimentally validated a method for measuring $k_{\vec{B}}$ and then applied the method to characterise $k_{\vec{B}}$ for three Roos chambers. The experimentally measured $k_{\vec{B}}$ for a PTW Farmer and Roos chamber was 0.993 ± 0.013 ($k = 1$) and 0.999 ± 0.014 ($k = 1$) respectively for a parallel MRI-linac at a beam quality of $TPR_{20/10} = 0.632$. Uncertainty was calculated as per table 1. Potential reasons for the large uncertainty and comparisons to previously published literature are discussed below.

Low B Field Location for chamber measurements

The minimal B field location had a field strength of 0.001 T. Positionally, the chamber can be set up within a 1 cm sphere at this point and be below 0.007 T. Our measurements are consistent with previously published simulations of the magnetic field for this magnet (Kolling *et al.*, 2013; Whelan *et al.*, 2018). If we can assume chamber response in the magnetic field is approximately linear relative

320   to field strength, as shown for Farmer-type chambers by Reynolds *et al.* (Reynolds *et al.*, 2013), then the difference between 0 T and 0.001 T is insignificant compared to the difference between 0.001 T and 1 T, which is the field strength at the isocentre of the MRI. Using the 0.001 T location to set-up a low field measurement point is a good approximation of 0 T and therefore will have minimal impact on chamber response when measuring $k_{\vec{B}}$. Positional changes within assumed set-up uncertainties, in

325   both the low and high measurement set-ups, will have minimal impact on the magnitude of the magnetic field at each position and therefore the collected charge.

Measurements of $k_{\vec{B}}$

Recombination and polarity measured for all chambers did not show any difference between the two magnetic field strengths. Jaffe plots over voltage ranges of 50 V – 300 V for the Farmer-type and 25 V

330   – 150 V for the Roos chambers confirm the applicability of the two-voltage method for measuring recombination at both low and high field strengths. This is consistent with previous measurements of ion recombination of a cylindrical chamber in a perpendicular MRI-linac, which was observed to have no significant change in ion recombination due to the magnetic field over a voltage range between 25 V – 400 V (Smit *et al.*, 2013).

335   The uncertainty calculated for $k_{\vec{B}}$ via table 1 is large compared to Monte Carlo simulations. This is primarily due to the large uncertainty in $N_{D,w,Q}^{Ref}$ for the reference chamber used at both 0 T and 1 T. The reproducibility of measurements, for both the reference chamber and field chamber, and reproducibility of the reference chamber contribute large relative uncertainties to the overall combined uncertainty. Because the measurements are at both 0 T and 1 T, the combined relative

340   uncertainty for the calculation of $k_{\vec{B}}$ is large. The quoted Type A uncertainty in $k_{\vec{B}}$ comes from the reproducibility of the three transfer sessions. Using this method to determine $k_{\vec{B}}$ for absorbed dose measurements will introduce large uncertainties in the measured dose.

The $k_{\vec{B}}$ measured for the PTW Farmer chamber in our work, 0.993 ± 0.013 (*k* = 1), showed good agreement with published Monte Carlo simulations in a parallel MRI-linac (Malkov and Rogers, 2018;

345   Spindeldreier *et al.*, 2017). Malkov and Rogers (Malkov and Rogers, 2018) simulated a $k_{\vec{B}}$ value of

0.9937 ± 0.0010 using a 1.5 T magnetic field and a 7 MV MRgRT photon spectrum (*TPR$_{20,10}$* = 0.695)

from the Elekta Unity (Elekta Solutions AB, Stockholm, Sweden). Spindeldreier *et al.* (Spindeldreier *et*

al., 2017) simulated a $k_{\vec{B}}$ value of 0.994 ± 0.003 using a 1.0 T magnetic field and a beam quality of

TPR$_{20,10}$ equal to 0.674. Previous measurements of the energy spectrum on the Australian MRI-linac

350   show a *TPR$_{20,10}$* value of 0.632 ± 0.007 (Begg *et al.*, 2019). Increased magnetic field strength results in

a larger $k_{\vec{B}}$ factor. (Spindeldreier *et al.*, 2017). Differences in beam quality have been shown to

introduce up to 0.5 % variation in $k_{\vec{B}}$ factors for cylindrical chambers on parallel MRI-linacs with lower

energy beams being impacted by the magnetic field to a larger extent (Malkov and Rogers, 2018). The

differences in simulated spectrums and magnetic field strengths highlight the need to verify simulated

355   values with measurements.

The measured $k_{\vec{B}}$ for the Roos chamber was similar to previously published Monte Carlo simulated

values at 0.35 T and 1.5 T (Malkov and Rogers, 2018). The Type A uncertainty in the average $k_{\vec{B}}$ value

of 0.2 % (*k* = 1) was no greater than the Type A uncertainty in the measured $k_{\vec{B}}$ for each individual

Roos chamber. The agreement in $k_{\vec{B}}$ observed across all Roos chambers is similar to the agreement in

360    $k_{\vec{B}}$ observed for Farmer-type chambers (Woodings *et al.*, 2019). Previous simulations of the Roos

chamber calculated a $k_{\vec{B}}$ correction factor of 0.9849 ± 0.001 using a 1.5 T magnetic field and beam

quality of *TPR$_{20,10}$* = 0.695, and 0.997 ± 0.001 using a 0.35 T magnetic field and beam quality of *TPR$_{20,10}$*

= 0.568 (Malkov and Rogers, 2018). Our measurement, 0.999 ± 0.014 (*k* = 1), agrees with the lower

beam quality and magnetic field strength simulation and is within 95 % confidence intervals for the

365   higher beam quality and field strength. Differences in magnetic field strength and beam energy have

an impact on the measured correction factor. As the magnetic field strength increases, the radius of

curvature of an electron in a magnetic field decreases meaning the air gap between the parallel plates

of the Roos chamber increases in significance as the field strength increases. Without further

simulations and/or measurements at different magnetic field strengths, the relationship between $k_{\vec{B}}$

370 and magnetic field is unknown. A correction factor close to 1.0 is expected for the Roos chamber because the predominately forward scattered electrons only have a small perpendicular component relative to the magnetic field. The stem material has been shown to impact $k_{\vec{B}}$ for cylindrical chambers (Malkov and Rogers, 2018). Finite element modelling of electrical fields inside the chamber has shown the impact of dead volumes on $k_{\vec{B}}$ for a cylindrical chamber (Pojtinger *et al.*, 2019). Further

375 simulations and modelling are required to investigate the impact of materials, the sensitive volume and the impact of the guard ring for parallel plate chambers in magnetic fields.

The methodology presented is similar to the ramp up/down method presented by Smit *et al.* (Smit *et al.*, 2013) and van Asselen *et al*. (van Asselen *et al.*, 2018). Our method has replaced the ramping up and down of the magnet with the ability to move the linac and dosimeter from a high to low field

380 measurement set-up. To the best of the authors' knowledge, no other MRI-linacs have the ability to move the linac from a high field to low field set-up.

Previous simulations of the magnetic field correction factor for a Roos chamber in perpendicular MRI-linacs have shown correction factors of between 8 % – 9 % (Pojtinger *et al.*, 2018; Malkov and Rogers, 2018). These simulated values, and an understanding of the electron paths for a wide air cavity such

385 as a parallel plate chamber, show the unsuitability of Roos chambers for absorbed dose determination in perpendicular MRI-linacs.

Rotational Response of the Roos Chamber

Reproducibility of the chamber response at 0°, for both the low and high field, was within ± 0.16 %. This places a limit on the ability to distinguish between response differences due to reproducibility or

390 chamber tilt. The response at an angle of ± 10° for both field strengths was consistent with the manufacturer recommendations for directional response (< 0.1 % for a ± 10° rotation(PTW, 2020)) noting the manufacturer recommendations were not in a magnetic field. The - 0.22 % difference relative to the average 0° value for the Roos 473 at - 10° was not thought to be significant. This is due to the relatively large tilt (10°) applied to the chamber which was easily observable as a set-up error.

395 The agreement between low and high field strengths within 0.2 % indicates that between face tilt angles of ± 30° there is no difference in the response caused by the magnetic field. This indicates that the magnetic field does not make the Roos chamber more susceptible to tilt set-up uncertainties. The measurements presented are in agreement with published simulations where no difference in the cavity dose to air was observed for parallel plate chambers with face tilts up to 3° relative to

400 simulations with no chamber tilt, in a parallel radiation and magnetic field (Malkov and Rogers, 2018).

Limitations and Future Work

The method used for measuring chamber correction factors relied on a cross-calibration from a chamber with a known dose to water calibration coefficient at both magnetic field strengths. This requires the chamber with the known magnetic field correction factor to have either been calibrated

405 in the magnetic field by comparison to a dosimeter with a known output in the magnetic field (alanine dosimetry (Billas *et al.*, 2017) or calorimetry (de Prez *et al.*, 2019)) or the chambers correction factor having been calculated via measurements with the magnetic field in a ramped up and down state (Smit *et al.*, 2013; van Asselen *et al.*, 2018). Future work will aim to develop an independent method to determine magnetic field calibration factors that does not depend on prior chamber calibration

410 factors.

An alternative method for determining $k_{\vec{B}}$, using similar measurements to those presented in this work, would be to transfer $k_{\vec{B}}$ from a chamber with a known $k_{\vec{B}}$ instead of using known $N_{D,w}$ values at both magnetic field strengths as presented in this work. If the known $k_{\vec{B}}$ was measured via a primary standard with a small uncertainty, then this could potentially reduce the uncertainty in the transferred

415 $k_{\vec{B}}$ depending on the uncertainty in the known $k_{\vec{B}}$. The additional uncertainty for long term chamber stability could be removed from the uncertainty budget. For the measurements presented, $k_{\vec{B}}$ would be calculated from the ratio of the $N_{D,w}$ values at both magnetic field strengths and thus no reduction in uncertainty would be achieved.

Parallel plate type chambers have not been previously recommended for photon beam reference dosimetry in dosimetry protocols (Andreo *et al.*, 2001). Recent measurements and simulations of the absorbed dose calibration factor with parallel plate type chambers indicate good agreement between measurements and simulations, however long-term chamber response stability remains an issue preventing the use of parallel plate type chambers for absorbed dose determination (Muir *et al.*, 2012). Our work shows a small $k_{\vec{B}}$ correction factor measured for the Roos chambers. Use of the Roos chambers to measure the absorbed dose on a parallel MRL would require either more frequent primary standard lab calibrations or a cross-calibration against a reference dosimeter on a conventional linac prior to absorbed dose determination on the parallel MRI-linac.

Measurement of the small correction factor for a parallel-plate chamber is important for future MRI-proton machines where a parallel orientation between the proton beam and magnetic field could be advantageous (Oborn *et al.*, 2017) and parallel plate chambers are a recommended dosimeter for absorbed dose determination (Andreo *et al.*, 2001).

Conclusion

This work presented measurements of the magnetic field correction factor, $k_{\vec{B}}$, for three Roos chambers at 1 T on a parallel MRI-linac. The measured $k_{\vec{B}}$ relied on the transfer of the dose to water calibration coefficient at both 0 T and 1 T from a calibrated chamber with a known $k_{\vec{B}}$. The methodology was validated by measuring the $k_{\vec{B}}$ for a PTW Farmer chamber and comparing to published simulations in the literature. The $k_{\vec{B}}$ for the PTW Farmer chamber at 1 T on a parallel MRI-linac was 0.993 ± 0.013 (k = 1). The average $k_{\vec{B}}$ factor measured for the three Roos chambers on a 1 T parallel MRI-linac was 0.999 ± 0.014 (k = 1). The beam quality used for the measurements of $k_{\vec{B}}$ was $TPR_{20/10}$ = 0.632. The small correction factor for the Roos chamber indicates that parallel plate type chambers are a suitable option for calibration of parallel MRI-linacs. The results have demonstrated a robust method for measuring magnetic field correction factors on a parallel MRI-linac.

Acknowledgement

References

Almond P R, Biggs P J, Coursey B M, Hanson W F, Huq M S, Nath R and Rogers D W 1999 AAPM's TG-51 protocol for clinical reference dosimetry of high-energy photon and electron beams *Med Phys* **26** 1847-70

Andreo P, Burns D, Hohlfeld K, Huq M, Kanai T, Laitano F, Smyth V and Vynckier S 2001 TRS-398: Absorbed Dose Determination in External Beam Radiotherapy: An International Code of Practice for Dosimetry based on Standards of Absorbed Dose to Water *International Atomic Energy Agency* **420**

Begg J, Alnaghy S J, Causer T, Alharthi T, George A, Glaubes L, Dong B, Goozee G, Keall P, Jelen U, Liney G and Holloway L 2019 Technical Note: Experimental characterization of the dose deposition in parallel MRI-linacs at various magnetic field strengths *Med Phys* **46** 5152-8

Bielajew A F 1993 The effect of strong longitudinal magnetic fields on dose deposition from electron and photon beams *Med Phys* **20** 1171-9

Billas I, Homer M and Duane S 2018 Report on dose measurements on the MRI-linac at Liverpool Hospital (Australia) performed by NPL

Billas I, Maughan D, Costa F, Perik T, Kaas J and Duane S *5th MR in RT Symposium, Sydney, Australia,2017),* vol. Series*)*

de Pooter J A, Billas I, de Prez L A, Duane S, Kapsch R P, Karger C, van Asselen B and Wolthaus J W H 2020 Reference dosimetry in MRI-linacs: evaluation of available protocols and data to establish a code of practice *Phys Med Biol*

de Prez L, Woodings S, de Pooter J, van Asselen B, Wolthaus J, Jansen B and Raaymakers B 2019 Direct measurement of ion chamber correction factors, k Q and k B, in a 7 MV MRI-linac *Phys Med Biol* **64** 105025

Fallone B G 2014 The rotating biplanar linac-magnetic resonance imaging system *Semin Radiat Oncol* **24** 200-2

Gargett M, Oborn B, Metcalfe P and Rosenfeld A 2015 Monte Carlo simulation of the dose response of a novel 2D silicon diode array for use in hybrid MRI–LINAC systems *Medical Physics* **42** 856-65

JCGM 2008 Evaluation of measurement data—guide to the expression of uncertainty in measurement *JCGM* **100** 1-116

Jelen U, Dong B, Begg J, Roberts N, Whelan B, Keall P and Liney G 2020 Dosimetric Optimization and Commissioning of a High Field Inline MRI-Linac *Frontiers in Oncology* **10**

Keall P J, Barton M, Crozier S and Australian MRI-Linac Program including contributors from Ingham Institute for Applied Medical Research, Illawarra Cancer Care Centre, Liverpool Hospital, Stanford University, Universities of Newcastle, Queensland, Sydney, Western Sydney, and Wollongong 2014 The Australian magnetic resonance imaging-linac program *Semin Radiat Oncol* **24** 203-6

Kolling S, Oborn B and Keall P 2013 Impact of the MLC on the MRI field distortion of a prototype MRI-linac *Medical Physics* **40** 121705

Lagendijk J J, Raaymakers B W and van Vulpen M 2014 The magnetic resonance imaging-linac system *Semin Radiat Oncol* **24** 207-9

Malkov V N and Rogers D W O 2018 Monte Carlo study of ionization chamber magnetic field correction factors as a function of angle and beam quality *Med Phys* **45** 908-25

Meijsing I, Raaymakers B W, Raaijmakers A J, Kok J G, Hogeweg L, Liu B and Lagendijk J J 2009 Dosimetry for the MRI accelerator: the impact of a magnetic field on the response of a Farmer NE2571 ionization chamber *Phys Med Biol* **54** 2993-3002

Muir B R, McEwen M R and Rogers D W 2012 Beam quality conversion factors for parallel-plate ionization chambers in MV photon beams *Med Phys* **39** 1618-31

Mutic S and Dempsey J F 2014 The ViewRay system: magnetic resonance-guided and controlled radiotherapy *Semin Radiat Oncol* **24** 196-9

O'Brien D, Roberts D, Ibbott G and Sawakuchi G 2016 Reference dosimetry in magnetic fields: formalism and ionization chamber correction factors *Medical Physics* **43** 4915-27

Oborn B M, Dowdell S, Metcalfe P E, Crozier S, Mohan R and Keall P J 2017 Future of medical physics: Real-time MRI-guided proton therapy *Med Phys* **44** e77-e90

Oborn B M, Ge Y, Hardcastle N, Metcalfe P E and Keall P J 2016 Dose enhancement in radiotherapy of small lung tumors using inline magnetic fields: A Monte Carlo based planning study *Med Phys* **43** 368

Pojtinger S, Dohm O S, Kapsch R P and Thorwarth D 2018 Ionization chamber correction factors for MR-linacs *Phys Med Biol* **63** 11NT03

Pojtinger S, Kapsch R P, Dohm O S and Thorwarth D 2019 A finite element method for the determination of the relative response of ionization chambers in MR-linacs: simulation and experimental validation up to 1.5 T *Phys Med Biol* **64** 135011

PTW 2020 PTW Dosimetry Roos Chamber Specifications.

Raaijmakers A J, Raaymakers B W and Lagendijk J J 2008 Magnetic-field-induced dose effects in MR-guided radiotherapy systems: dependence on the magnetic field strength *Phys Med Biol* **53** 909-23

Reynolds M, Fallone B G and Rathee S 2013 Dose response of selected ion chambers in applied homogeneous transverse and longitudinal magnetic fields *Med Phys* **40** 042102

Reynolds M, Rathee S and Fallone B G 2017 Technical Note: Ion chamber angular dependence in a magnetic field *Med Phys* **44** 4322-8

Roberts N F, Patterson E, Jelen U, Causer T, Holloway L, Liney G, Lerch M, Rosenfeld A B, Cutajar D and Oborn B M 2019 Experimental characterization of magnetically focused electron contamination at the surface of a high-field inline MRI-linac *Medical Physics* **46** 5780-9

Smit K, van Asselen B, Kok J G, Aalbers A H, Lagendijk J J and Raaymakers B W 2013 Towards reference dosimetry for the MR-linac: magnetic field correction of the ionization chamber reading *Phys Med Biol* **58** 5945-57

Spindeldreier C K, Schrenk O, Bakenecker A, Kawrakow I, Burigo L, Karger C P, Greilich S and Pfaffenberger A 2017 Radiation dosimetry in magnetic fields with Farmer-type ionization chambers: determination of magnetic field correction factors for different magnetic field strengths and field orientations *Phys Med Biol* **62** 6708-28

van Asselen B, Woodings S J, Hackett S L, van Soest T L, Kok J G M, Raaymakers B W and Wolthaus J W H 2018 A formalism for reference dosimetry in photon beams in the presence of a magnetic field *Phys Med Biol* **63** 125008

Whelan B, Kolling S, Oborn B M and Keall P 2018 Passive magnetic shielding in MRI-Linac systems *Phys Med Biol* **63** 075008

Woodings S J, van Asselen B, van Soest T L, de Prez L A, Lagendijk J J W, Raaymakers B W and Wolthaus J W H 2019 Technical Note: Consistency of PTW30013 and FC65-G ion chamber magnetic field correction factors *Med Phys* **46** 3739-45

Appendix 1: Details on $N_{D,w}$ *Transfer Uncertainty*

Appendix Table 1: Combined relative standard uncertainty of the $N_{D,w}$ transfer at both 0 T and 1 T for the PTW Farmer and Roos chambers.

Component of Uncertainty	PTW Farmer		Roos	
	0 T	1 T	0 T	1 T
Type A				
Reproducibility of measured charge for reference chamber[1]	0.04	0.04	0.04	0.04
Reproducibility of measured charge for field chamber[1]	0.05	0.05	0.06	0.06
Type B				
Uncertainty in $N_{D,w,Q}^{Ref}$ for reference chamber at beam quality Q	0.7[#]	1.0[&]	0.7[#]	1.0[&]
Positioning of reference chamber at correct depth[2]	0.1	0.1	0.1	0.1
Positioning of field chamber at correct depth[2]	0.1	0.1	0.1	0.1
Water tank setup (± 1 mm)[3]	0.1	0.1	0.1	0.1
Stability of reference chamber over time[4]	0.3	0.3	0.3	0.3
$k_{T,P}$ correction[5]	0.05	0.05	0.05	0.05
k_{pol} - reference chamber[6]	0.05	0.05	0.05	0.05
k_s - reference chamber[6]	0.1	0.1	0.1	0.1
k_{pol} - field chamber[6]	0.05	0.05	0.05	0.05
k_s - field chamber[6]	0.1	0.1	0.1	0.1
k_{rp} - Radial Profile or Volume Averaging Difference[7]	0	0	0.2	0.2
k_{leak} - leakage current	0.05	0.05	0.01	0.01
Combined Relative Standard Uncertainty (*k* = 1)	0.8 %	1.1 %	0.83 %	1.1 %

540 1. Reproducibility of the reference chamber (FC65-G) and field chambers (PTW30013 and 3 x Roos chambers) was assessed via the maximum percentage uncertainty observed over three separate measurements (StdDev/Mean for each measurement) at each magnetic field strength. The value combines the uncertainty in the chambers and a CC13 reference chamber. The cc13 chamber was used to address output stability of the linac.

545 2. Depth uncertainty was a combination of wall thickness measurement, depth position tool length, depth position set-up reproducibility and chamber cap thickness (0.1 %, <0.1 %, 0.2 % and 0.06 % respectively). Wall thickness, depth position tool length and cap thickness uncertainty was the smallest increment of a vernier calliper. Combined uncertainty equals 0.23 % which at 100 mm depth is 0.23 mm. At a depth of 100 mm on the AusMRL the PDD gradient is

550   0.4 %/mm. Therefore an uncertainty of 0.23 mm translates to an uncertainty of 0.1 %.

3. SSD of tank set-up is ± 1 mm. At SSD of 1732 mm, inv sqr law for 1 mm is 0.1 %. Tank set-up not changed between different chambers therefore uncertainty only included once in $N_{D,w}$ Transfer uncertainty.

4. Stability of the chamber over time was assessed via Strontium 90 checks. Long term stability of chamber response was 0.3 %. AAPM TG51 (Almond *et al.*, 1999) recommends using Co60 not strontium 90. However, that is not available. Applied to both 0 T and 1 T measurements as each $N_{D,w}$ transfer has an uncertainty due to the stability of the chamber.

5. Chambers were kept in the water phantom for the duration of the measurements to ensure thermal equilibrium with the water. Only resolution uncertainties in the thermometer (Resolution = 0.1°C therefore ± 0.05°C) and barometer (Resolution = 0.1 kPa therefore ± 0.05 kPa) where included as the same thermometer and barometer were used at 0 T and 1 T for $N_{D,w}$ transfer measurements and thus calibration uncertainties will cancel out. The uncertainties of ± 0.05°C and ± 0.05 kPa corresponded to 0.02 % and 0.05 % respectively. Combined in quadrature this becomes 0.05 %.

6. k_{pol} and k_s uncertainty based on AAPM TG51 (Almond *et al.*, 1999) addendum values.

7. Volume averaging difference not applicable between Farmer-type chambers as Farmer-type chambers were placed in the same location. Between Farmer-type and Roos chamber the largest difference in calculated k_{vol} was 0.2 %. This was due to the FFF beam being at an extended distance and the dose deposition curve was relatively flat. An estimation of the uncertainty of 0.2 % is used.

8. Leakage current was corrected for at electrometer with leakage less than 0.1 % of signal. Therefore associated uncertainty was set at 0.05 % as per AAPM TG51 (Almond *et al.*, 1999) addendum for cylindrical chambers and 0.01 % for plane parallel chambers as per Muir *et al.* *(Muir et al., 2012)*

\#   From NPL FFF Calibration report for farmer chambers (*k* = 1)

\&   From NPL Internal Report 46 (Billas *et al.*, 2018)